

EFFECT OF PRINT BED'S HEAT FLOW ON CURLING AND SURFACE ROUGHNESS OF FDM-PRINTED ABS SAMPLE

Kok-Tee Lau*, Mastura Mohammad Taha, Syahibudil Ikhwan Abdul Kudus, See Ern Chung

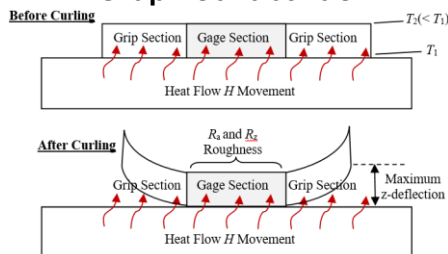
Fakulti Teknologi Kejuruteraan Mekanikal dan Pembuatan, Universiti Teknikal Malaysia Melaka, Hang Tuah Jaya, 76100 Durian Tunggal, Melaka, Malaysia

Article history

Received
7 May 2022
Received in revised form
4 September 2022
Accepted
13 October 2022
Published Online
23 February 2023

*Corresponding author
ktlau@utem.edu.my

Graphical abstract



Abstract

The optimization of printing parameters, in particular the print bed aspect, is essential for the further improvement of print quality. This paper investigates the effect of the print bed's heat flow and surface properties (i.e. materials and surface roughness) on the curling defect and surface roughness of the ABS-based dog bone designed print. The print bed temperature is varied, and the corresponding heat flow is measured using a portable heat flow meter. The maximum z deflection (curling) of the print is characterized using Geomagic Control X metrology software by measuring the dimension deviation of the 3D scanned print compared with the CAD drawing. The surface roughness in terms of the R_a and R_z of the print are obtained by a stylus-based contact profilometer. The measured heat flow data have a positive linear correlation with the print bed temperature, which is confirmed by our theoretical calculation. The surface roughness of the print is higher when printed on the zinc plate-overlaid print bed, compared with the standard (unmodified) print bed. Furthermore, the applied heat flow has a large positive correlation with the print's roughness but no correlation with the maximum z deflection. The roughness and z-deflection behaviour are attributed to the curling at the grip section of the print, resulting in a shorter interaction time with the print bed surface compared with the gage section that remains in physical contact throughout the 3D printing.

Keywords: Additive manufacturing, fused deposition modelling (FDM), acrylonitrile-butadiene-styrene (ABS), 3D laser scanner, dimensional accuracy

Abstrak

Pengoptimuman parameter pencetakan khususnya aspek katil cetakan adalah penting untuk penambahbaikan lagi kualiti cetakan. Makalah ini cuba menyiasat kesan aliran haba katil cetakan dan sifat permukaan (i.e. kekasaran dan bahan permukaan) keatas kecacatan lencong dan kekasaran permukaan cetakan berasaskan ABS. Suhu katil cetakan dipelbagaikan dan nilai aliran haba yang sepadan diukur menggunakan meter aliran haba mudah alih. Pesongan-z maksimum (kerutan) cetakan telah dicirikan menggunakan perisian metrologi Geomagic Control X dengan mengukur sisihan dimensi cetakan imbasan 3D berbanding lukisan CAD. Manakala, kekasaran permukaan dari segi R_a dan R_z cetakan diperolehi oleh profilometer sentuhan berasaskan stylus. Data aliran haba mempunyai korelasi positif dan linear dengan suhu katil cetakan, yang disahkan oleh pengiraan teori kami. Kekasaran permukaan cetakan adalah lebih tinggi apabila dicetak pada katil cetakan bertindih plat zink berbanding dengan katil cetakan piawaian (tidak diubah suai). Tambahan pula, aliran haba yang digunakan mempunyai korelasi yang besar dan positif dengan kekasaran

cetakan, tetapi tiada korelasi ditunjukkan dengan pesongan-z maksimum. Kelakuan kekasaran dan pesongan z adalah disebabkan oleh lengcongan pada bahagian pengkaman cetakan menghasilkan masa interaksi yang lebih singkat dengan permukaan katil cetakan berbanding dengan bahagian tolok yang kekal dalam sentuhan fizikal sepanjang proses pencetakan 3D.

Kata kunci: pembuatan aditif, pemodelan pemendapan bersatu (FDM), akrilonitril–butadiena–stirena (ABS), pengimbas laser 3D, ketepatan dimensi.

© 2023 Penerbit UTM Press. All rights reserved

1.0 INTRODUCTION

In recent times, 3D printing or additive manufacturing in an industrial term is a rapidly growing technology. As some key patents related to the technologies expired, home-market printer prices, particularly regarding fused deposition modelling (FDM) dropped tremendously [1]. The reduced price of 3D printing technologies, especially the polymer-based FDM printer, made these technologies increasingly accessible to the public [2].

Recent research in FDM technologies have been shifting more towards the study on the optimization of Design for Manufacturing to improve the dimension accuracy [3-5] and surface quality [6, 7] of the printed part, with a less focus towards the optimization of the printing parameters. These are particularly correct for the FDM technologies involving the usage of established, commercially available feedstock materials such as acrylonitrile butadiene styrene (ABS) and polylactic acid (PLA). Nevertheless, the development of new composite materials for the FDM feed stock creates a new challenge to match the similar quality of printing by established materials. For example, graphene-doped PLA nanocomposite printing is unable to produce quality prints on a non-heated print bed, though this setting has been used without issue for pure PLA printing [7].

The optimization of FDM printing parameters is essential for the improvement of print quality aspects. Nevertheless, very minimal attention has been paid to understanding the role of the heated print bed's heat flow role on the print quality. To date, most discussions have focused on the effect of the print bed temperature on the adhesion of the initial print layer and the detrimental effect of poor adhesion on the dimension integrity of the print [8, 9]. Furthermore, understanding the fundamental heat flow behaviour of the print bed on the print is vital as concerns in regard to print bed technologies have been tweaked and in some cases have not yet been invented for new areas of supply chains such as metal-powder companies, medical supply houses and recyclers [1].

This paper investigates the effect of the print bed's heat flow and surface properties (i.e. materials and surface roughness) on the curling defect and surface roughness of the ABS-based dog bone designed print.

The methodology approach to modify the print bed's heat flow was by overlaying an additional thermal conductive zinc plate onto the standard print bed (in as-received form) to modify the heat flow condition of the print bed surface. Examining the effect of surface interaction between the FDM printed sample and the print bed surface is beyond the scope of this paper.

2.0 METHODOLOGY

2.1 CAD Development

Firstly, the solid model of the specimen was sketched using SolidWork. The dog-bone-shaped design was based on the dimensions of ASTM D638-10, type I standard tensile specimen (illustrated in Figure 1). Then, the solid model was sliced using a 3D printer slicer software called Flashprint to create G-code language to control 3D printing path. During the slicing stage, the 3D printer parameters were defined (details in Table I).

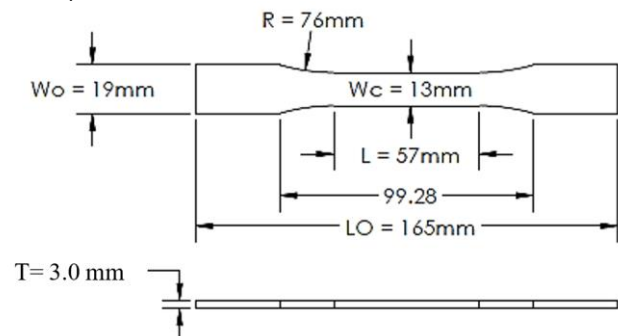


Figure 1 Specimen's dimensional profile based on ASTM D638-10 type I standard. W_c and W_o are the width of the gage section and the grip section, respectively

Table 1 Parameter setting for 3D printer slicer software

Parameter	Setting Value
Infill density (%)	20
Infill pattern	Hexagon
Layer temperature (°C)	220
Printing speed (mm/s)	60
Layer height (mm)	0.18
Print bed Temperature (°C)	100, 105, 110, 115, 120

2.2 Printing of Sample

The sample was printed using Flashforge Creator Pro model FDM printer machine (printing area = 225 mm × 145 mm × 150 mm, print bed materials = aerospace-graded aluminium covered with Flashforge build surface sticker, print bed thickness = 6.3 mm). ABS filament (blue, diameter = 1.75 mm, 1 kg, 3D Printing Canada) was used as the feed stock material. Printing was performed on a standard (unmodified print bed; as-received from manufacturer) and zinc plate-overlaid print bed surface at print temperatures of 100 °C, 105 °C, 110 °C, 115 °C and 120 °C. The selected temperatures were the practical temperature range of the print bed [9]. Three print specimens were fabricated for each parameter to provide the variability data. Sample size was limited to three specimens to reduce total printing time and to minimize the risk of environmental error. Each printing was performed in an open setup where the printed specimen was exposed to ambient temperature and humidity (i.e. air-conditioned environment).

Table 2 compares the surface properties (i.e. thickness, R_a , R_q and R_z roughness) of the Flashforge Build Surface Sticker (i.e. applied on the standard print bed) and zinc plate (i.e. used for zinc plate-overlaid print bed). The thicknesses of the Flashforge Build Surface Sticker and the zinc plate were determined using a Vernier-scaled outside micrometre (Mitutoyo), whereas their surface roughness were measured by a standard profilometer (skidless-typed stylus, model: SJ-401, Mitutoyo) based on ISO4287:1997 standard. Three

readings were obtained for each surface roughness measurement.

The zinc plate-overlaid print bed was set up by overlaying a commercially available zinc plate (dimension = 232 mm × 154 mm, galvanized iron) on top of the standard print bed to alter the original heat flow condition. The zinc plate was fastened on the standard print bed using a commercially available thin double-sided tape to ensure a full physical contact. The FDM's built-in distance sensor could determine the initial distance between the nozzle head and the print bed surface; thus, it was able to cancel the added height contributed by the zinc plate overlaid on the standard print bed. After the completion of each printing, the printed samples were removed carefully using a commercially available cutter knife and then cooled to room temperature before storage. Figures 2 (a) and 2 (b) show the images of two finished printed specimens on the standard and zinc plate-overlaid print bed, respectively.

Table 2 Properties of print bed surface

Surface Property	Print Bed Surface Type	
	Flashforge Build Surface Sticker (Standard)	Zinc Plate overlaid (Zinc-overlaid)
Material	Plastic Sheet	Commercial Galvanized Iron
Thickness (mm)	0.156 (including 3M 9080 adhesive layer)	0.140
R_a (μm)	9.357±0.024	0.061±0.006
R_q (μm)	11.473±0.282	0.083±0.014
R_z (μm)	46.337±2.121	0.546±0.165

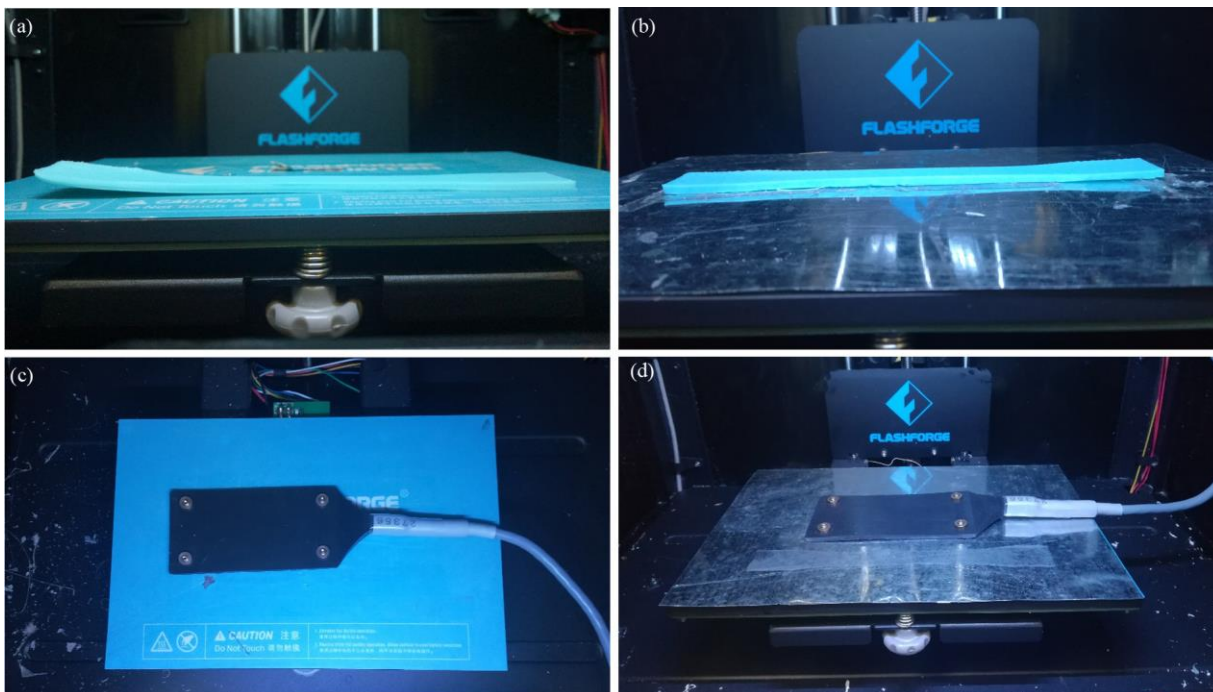


Figure 2 Photo images (a) and (b) show the printed specimen on a Standard (unmodified), and Zinc plate-overlaid print beds respectively. Photo images (c) and (d) show heat flow measurement setup on both print beds prior to printing

2.3 Heat Flow Measurement

Heat flow was measured using a portable heat flow meter (model: HFM201, Teledyne Hastings Instruments) on the empty standard and zinc plate-overlaid print bed prior to specimen printing (the measurement setup is illustrated in Figures 2 (c) and (d)). For the first heat flow measurement on each print bed type, the print bed was set at the required temperature for 15 min to stabilize the print bed temperature. After a new print bed temperature was set for the print bed type, only 5 min waiting time was applied before the heat flow measurements.

2.4 3D Dimension Scanning and Correction

Printed samples were scanned using 3D scanner machine (scanning precision = 0.0749 mm, model: Rexscan CS2, Solutionix). The obtained 3D scan data were refined by Materialise Magics and Polywork software. The refinement was required on a small portion of the scan data that was missing due to factors such as scanned sample preparation and limitation of the scanner for thin sample scanning.

2.5 Surface Roughness Measurement

The surface roughness on the upskin of the printed samples was measured using the profilometer

mentioned in Section 2.2. Measurements were performed on the planar upskin surface at the gage section. Measurements from three specimens printed by similar printing parameters were used to calculate the average and standard deviation for R_a and R_z data points and the error bars.

2.6 Maximum z-Deflection Measurement

Then, the dimensions provided by the scan data of the printed sample were compared with the sample's Solidwork CAD dimensions using Geomagic Control X metrology software. During the comparison, the z deflection of the scan data from the Solidwork 2D dimensions at the sample's symmetrical plane viewed from the y axis was measured (see Figure 3). The maximum z deflection was used as the data point to represent the sample's degree of curling, whose dimension was defined by Schmutzler et al. [10]. The standard deviation data were used to plot the error bars of the data points. Armillotta et al. showed that the curling mode along the z direction was most dominant along the x-z (longitudinal) plane for the long and thin sample's dimensions [11].

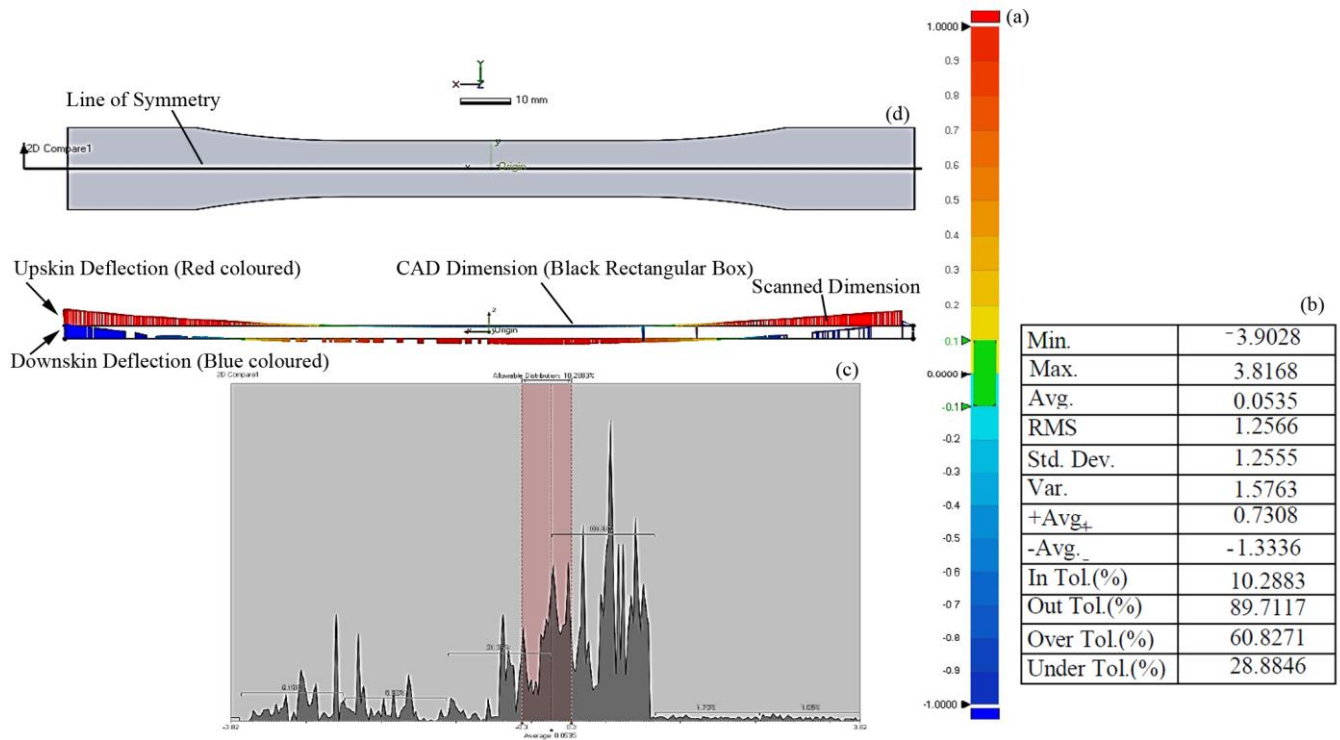


Figure 3 Side view of zinc plate-overlaid sample printed at a print bed temperature of 120 °C shows z deflection along the sample's symmetrical plane. Insert: (a) z deflection to colour scale bar in mm, (b) z-deflection statistical data, (c) z-deflection histogram and (d) front view of the samples

2.7 Statistical Analysis

Statistical analyses at 95% confidence were conducted using the Data Analysis ToolPak add-in of

MS Excel 2016 [12, 13]. Univariate regression analyses were conducted on the maximum z deflection and surface roughness data as functions of heat flow to determine if the obtained regression coefficients

were statistically significant. Next, t-test analyses were conducted on standard and zinc plate-overlaid sample groups to determine if their maximum z deflection and surface roughness data were significantly different. For the data plots that exhibited statistically significant regression coefficients, linear fits with the respective trendline equations and R squared of linear fit (R^2) were generated using ordinary least square technique. The studied maximum z deflection and surface roughness data were assumed to exhibit normal distribution behaviour.

3.0 RESULT AND DISCUSSION

Heat flow measurement was used in the current study to represent the effect of print bed temperature. The former was used because the heat flow generated from the print bed surface was more accurately represented by the direct measurement on the print bed surface, which was in direct contact with the initial print layer, particularly for the print bed overlaid with zinc plate. Heat flow data show a strong correlation with the increasing print bed temperature for both the standard and zinc plate-overlaid print bed (see Figure 4). However, the heat flow values detected on the surface of the zinc plate-overlaid print bed were lower than on the standard print bed at the same print bed temperature. Their heat flow difference increased from 10% at 100 °C to 48% at 120 °C.

However, the heat flow increases on the zinc plate surface still maintained a positive linear relationship with the print bed temperature. The increase percentage of the heat flow difference between the two print beds could be due to the increasing heat loss from the high-thermal-

conduction zinc plate to the surroundings through radiation and convection.

The relationship of heat flow and print bed temperature was derived based on the heat flow mechanism, as illustrated in Figure 5. When the printing was completed, a continuous heat flow from the surface of the high-temperature print bed to the downskin (initial layer) of the printed sample was observed. The downskin of the printed sample was presumed maintained at the same temperature as the print bed's surface, irrespective of the type (standard or zinc overlaid print bed), because of direct thermal contact. However, a temperature gradient was immediately formed between the opposite surfaces of the ABS print, in which the upskin's temperature became lower than the print bed's temperature. This outcome was likely because of the poor heat conduction of the sample material and the continuous heat loss from the print's top layer through the convection mechanism. Thermal conduction was the dominant heat flow mechanism at the interface of the print bed and the printed specimen due to the continuous physical contact between them throughout the printing. The thermal conductivity of the ABS print was extremely low (i.e. 0.19 W/m °C [14]) compared with the thermal conductivities of the print bed materials that were estimated at 51.9 and 121 W/m °C for the zinc plate and aluminium alloy 2024, respectively [15].

Based on the proposed heat flow mechanism, heat flow H (unit in W/m²) related to heat transfer Q (unit in J) was derived by the following equation [16]:

$$Q = HA\Delta t, \quad (1)$$

where A (unit in m²) is the area of the thermal contact surface, and Δt is the time interval of the heat flow measurement.

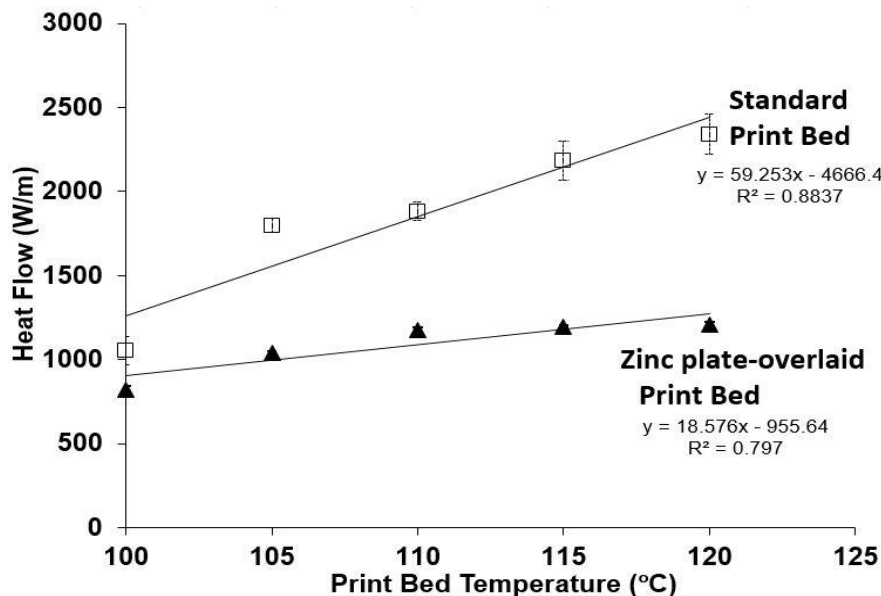


Figure 4 Applied Heat flow as function of print bed temperature for two types of print bed

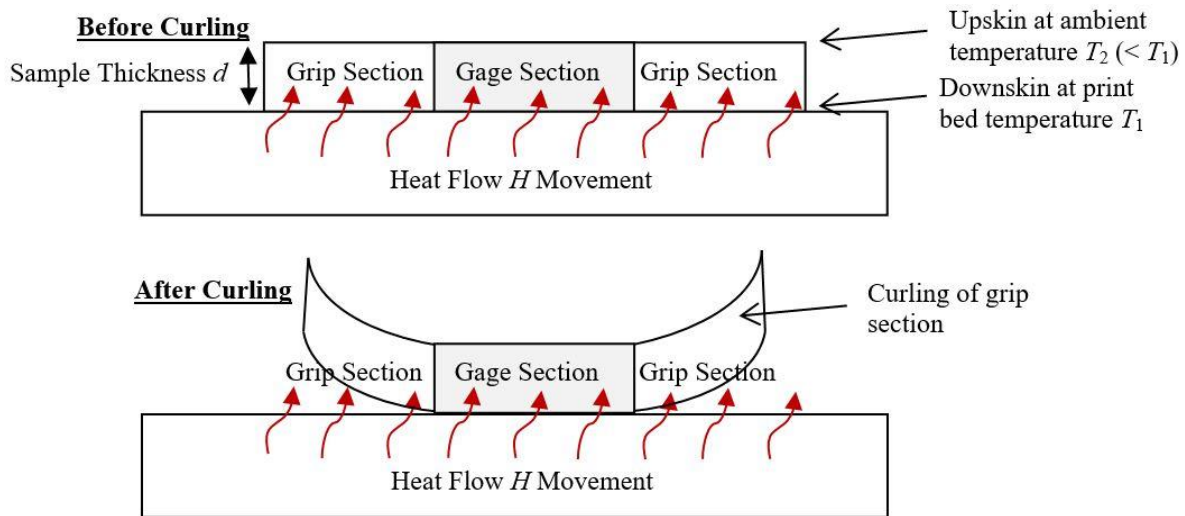


Figure 5 Schematic of heat flow mechanism from print bed to the printed sample before and after the curling of sample

Subsequently, the heat transfer term of Equation 1 can be substituted by the law of heat conduction (Fourier's law) as follows [16, 17]:

$$\frac{kA\Delta T}{d} = H\Delta t, \quad (2)$$

where ΔT (unit in $^{\circ}\text{C}$) is the temperature gradient between the initial layer and the top layer of the printed sample area of the thermal contact surface, Δt (unit in s) is the time interval of the heat flow measurement and k (unit in $\text{W/m } ^{\circ}\text{C}$) is the thermal conductivity of the print.

Then, ΔT is substituted with $T_1 - T_2$, the temperature of the downskin and upskin of the print, respectively. The surface areas A of the downskin and upskin are the same. Thus, these variables on both sides of Equation 2 are cancelled, resulting in a simpler equation:

$$\frac{k\Delta(T_1 - T_2)}{d} = H\Delta t \quad (3)$$

If the top layer's temperature T_2 is presumed constant due to the unchanged ambient

environment and specimen design, Equation 3 clearly shows that the applied heat flow value H is linearly proportional to the print bed temperature T_1 , thus validating the linear correlation of the experimental data illustrated in Figure 4.

Print curling occurred before the printing was completed. The curling feature was clearly shown on both standard and zinc plate-overlaid specimens, as shown in Figures 2 (a) and (b). The measurement of the maximum z deflection on the upskin of the curled samples showed a strong linear correlation with the increasing maximum z deflection on the downskin of the same curled samples obtained either from the standard or zinc plate-overlaid print bed (see Figure 6). Table 3 lists the heat flow, minimum and maximum z -deflection data corresponding to the respective print bed temperatures. Figure 6 clearly shows that the curling measured at the downskin of the studied curled samples increased proportionally with the curling measured on the upskin of the same samples. This behaviour was similarly shown on the samples printed on the zinc plate-overlaid print bed.

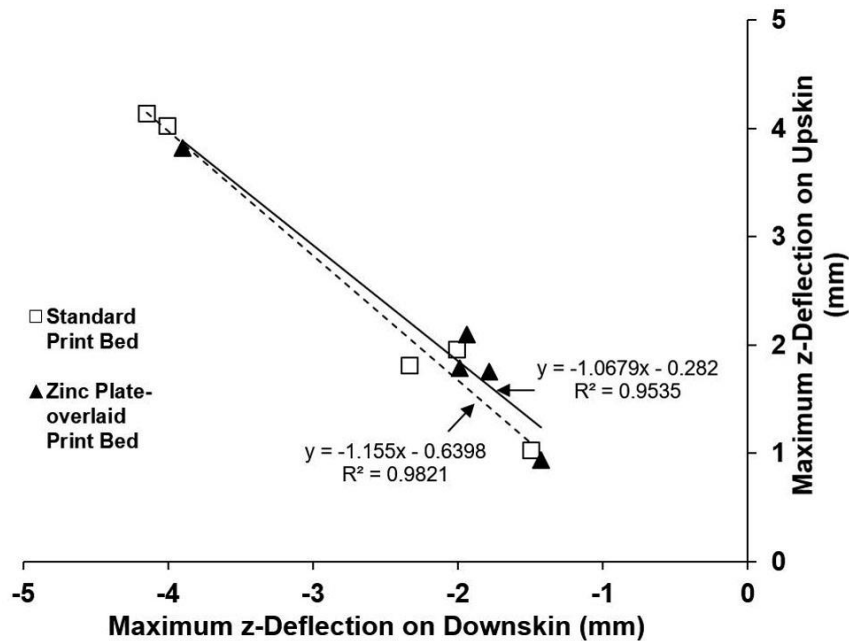


Figure 6 Upskin's maximum z deflection as a function of downskin's maximum z deflection for samples printed at a print bed temperature range of 100 °C–120°C

Table 3 Heat flow and z-deflection data at different print bed temperatures and surfaces

Print Bed Temperature (°C)	Heat Flow (W/m)		Min. z-Deflection (mm)		Max. z-Deflection (mm)	
	Standard	Zinc Plate overlaid	Standard	Zinc Plate overlaid	Standard	Zinc Plate overlaid
100	1052±83	818±21	-1.4960	-1.4261	1.0286	0.9347
105	1798±40	1042±10	-2.0058	-1.9866	1.9545	1.7843
110	1883±56	1177±13	-4.1455	-1.7859	4.1383	1.7507
115	2185±116	1196±7	-4.0058	-1.9402	4.0221	2.0949
120	2339±119	1206±18	-2.3312	-3.9028	1.8097	3.8168

Figure 7 shows the plot of the upskin's maximum z deflection as a function of applied heat flow for both samples. The increasing heat flow may increase the maximum z deflection of the sample. However, the regression analysis on the upskin's maximum z deflection as a function of applied heat flow shows regression coefficients for the standard and zinc plate-overlaid samples were statistically insignificant (see Appendix A). The results were unable to conclude if the applied heat flow (or print bed temperature) significantly influenced the change of the sample's maximum z deflection. Rosli *et al.* also reported a thin printed sample is less affected by the variation of print bed temperature compared with a thick sample [18].

The t-test analysis on both standard and zinc plate-overlaid sample data showed that their sample means were not significantly different (see Appendix B). This finding implies the noncorrelation between heat flow and maximum z deflection was not likely affected by the print bed type or the addition of an overlay on the standard print bed. This finding shows the ABS curling could not be solely controlled by applied heat flow (related to print bed temperature).

The findings from the regression and t-test analyses need to be interpreted with caution

because of the large data point error of Figure 7. The visual observation on the curling structure of the printed specimen after printing demonstrated a prominent curling on one end of the dog-bone-shaped specimen, as shown in Figures 2(a) and (b). The curling error may be caused by the print bed levelling factor. Nevertheless, the curling issue was only observed at the grip section and did not affect the gage section, the area where surface roughness was measured.

The regression analysis on the upskin's R_a roughness as a function of applied heat flow (refer Figure 8) showed regression coefficients for the standard and zinc plate-overlaid samples were statistically significant (p value < 0.05). The R_a roughness increased slowly but steadily with the increasing applied heat flow (i.e. increasing print bed temperature). The R_z roughness data of the standard samples also exhibited a similar positive correlation with the increasing heat flow (see Figure 9). The regression analysis on the upskin's R_z roughness as a function of applied heat flow showed regression coefficients for the standard samples were statistically significant (p value < 0.05). However, the correlation between R_z roughness and heat flow of the zinc plate-overlaid adhesive samples was not

statistically significant (p value > 0.05). The dependence of R_z roughness on heat flow, which was more sensitive to roughness spike [19], confirmed the R_a finding regarding the print's roughness dependence on the applied heat flow.

Study on print bed temperature dependence roughness result has not previously been reported. However, recent studies have been conducted on the temperature effect before and after specimen printing. Pérez *et al.* reported no clear influence of printing temperature (at extrusion component) on surface roughness [20]. Jo *et al.* showed that the surface roughness of the FDM print reduced after post printing reflow treatment at 160 °C [21, 22]. Engagingly, our finding clearly showed that the zinc plate-overlaid samples' surface demonstrated a higher R_a roughness than the standard samples. The former exhibited a higher R_a roughness value and a larger gradient (R value) as a function of heat flow than the latter. The surface interaction between the print and the zinc plate-overlaid surface occurred during printing, resulting in a different specimen surface texture.

Contrary to the maximum z-deflection data, the surface roughness of the standard and zinc plate-overlaid samples showed a significantly strong correlation with the applied heat flow value. A possible explanation is the strong influence of the heat flow on the surface roughness because the gage section of both standard and zinc plate-overlaid dog bone-shaped samples were maintained in tight physical contact with the print bed throughout the printing. Unlike the gage section, both ends of the dog bone specimen's grip section were curled away from the print bed surface during the printing. Under this condition, the gage section experienced a better thermal contact than the grip section due to the former's good physical contact under a longer duration. Thus, the heat flow of the print bed had a far more significant influence on the surface roughness (R_a and R_z roughness) of both standard and zinc plate-overlaid samples. The lower interaction time of the grip section with the print bed due to the print's curling also explained the lack of z-deflection data dependence on the heat flow value, as stated earlier.

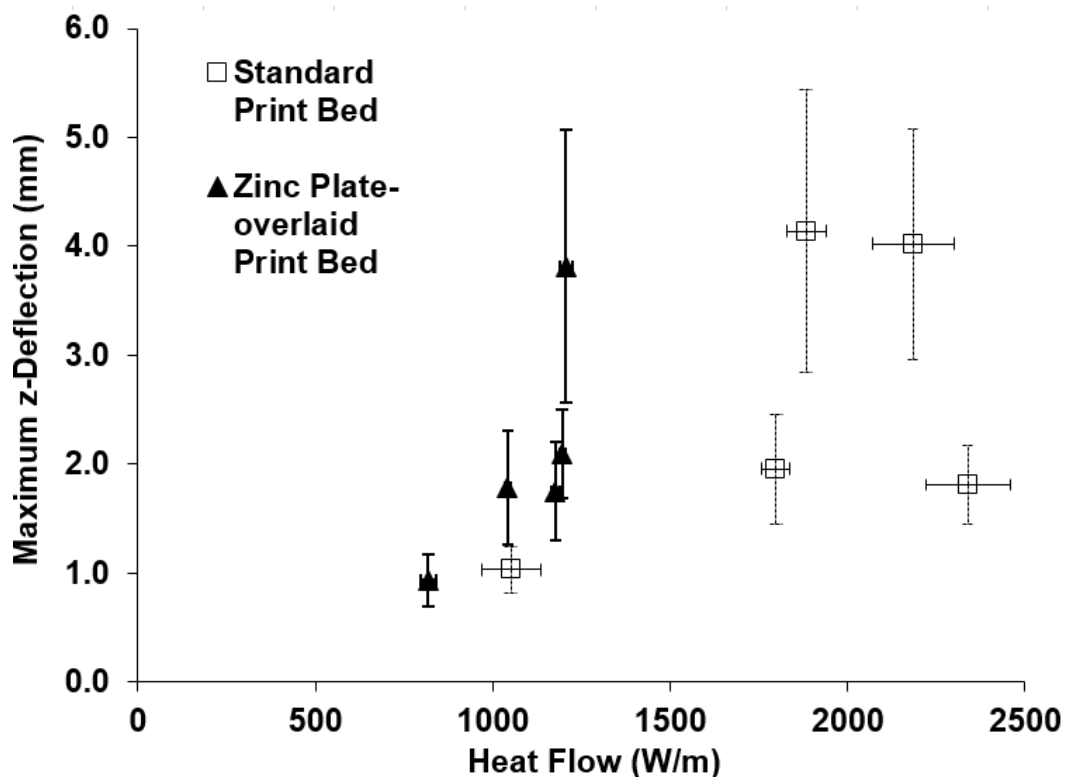


Figure 7 Upskin's maximum z deflection as a function of applied heat flow or samples printed at a print bed temperature range of 100 °C–120 °C

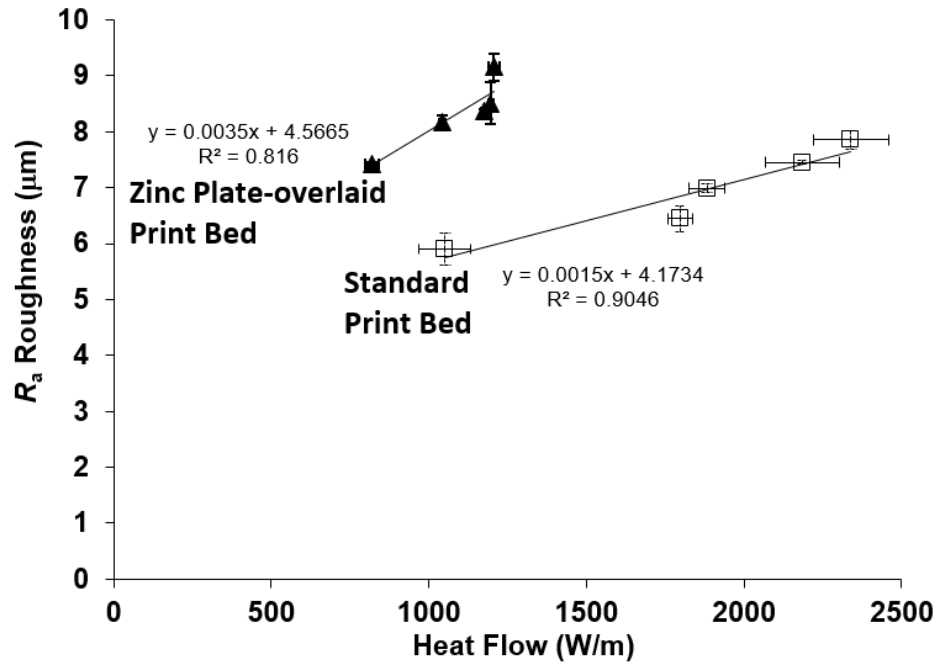


Figure 8 R_a roughness of printed samples as a function of applied heat flow

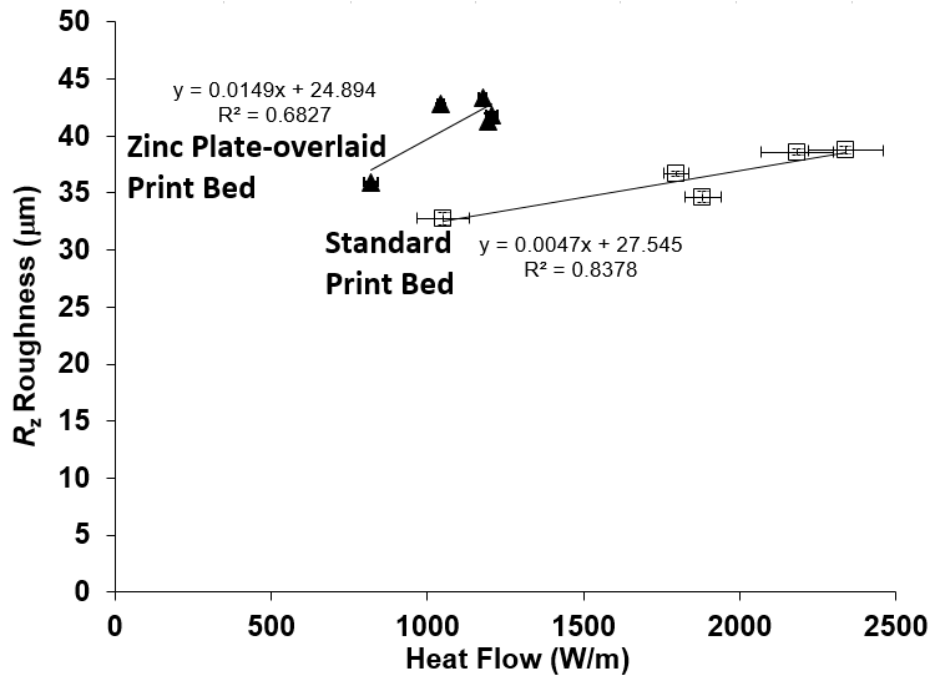


Figure 9 R_z roughness of printed samples as a function of applied heat flow

4.0 CONCLUSION

This paper demonstrated through theoretical calculations a linear relationship of the print bed temperature with the heat flow applied to the print during FDM printing. Furthermore, the experimental study showed that the R_a and R_z roughness of the print increase with the rise of applied heat flow (print bed temperature). Regarding the effect of print bed

surface property, the surface roughness of the zinc plate-overlaid sample was higher than that of the standard sample. However, this paper was unable to show any correlation between the applied heat flow and the maximum z deflection (also known as curling) of the print on both standard and zinc plate-overlaid print beds. A further research should focus on printing on a print bed with a lower heat flow condition (print bed temperature) to reduce the

curling and surface roughness of the ABS print, in particular the FDM technique. Nevertheless, curling data errors caused by FDM setup need to be reduced through the improvement of print bed levelling. Mechanical properties can be conducted if large curling and roughness are solved.

Acknowledgement

The authors are grateful to the Ministry of Education Malaysia for supporting this work under grant no.: FRGS/1/2022/FTKMP/F00523. The authors wish to acknowledge technical staff of Fakulti Teknologi Kejuruteraan Mekanikal dan Pembuatan for the technical supports in FDM printing, 3D scanning, software accessibility and surface roughness measurement.

References

- [1] Jordan, J. M. 2019. *3D Printing*. Cambridge: MIT Press. Doi: <https://doi.org/10.7551/mitpress/11800.001.0001>.
- [2] Taha, M. M., Jumaidin, R., Razali, N. M. and Kudus, S. I. A. 2020. Green Material For Fused Filament Fabrication: A Review. In Mastura, M. T. and Sapuan, S. M. (eds.). *Implementation and Evaluation of Green Materials in Technology Development: Emerging Research and Opportunities: Emerging Research and Opportunities*. Hershey: IGI Global.
- [3] Ranganathan, R., Ravi, T. and Pugalandhi, A. 2019. Analysis of Shrinkage Compensation Factor (SCF) of FDM uPrint SE for Accuracy Enhancement. *International Journal of Integrated Engineering*. 11(1): 207-16. Doi: <https://doi.org/10.30880/ijie.2019.11.01.022>.
- [4] Maidin, N. A. 2020. Design for Manufacturability (DFM) of 3D Printed Parts Fabricated Using Open Source 3D Printer. *International Journal of Integrated Engineering*. 12(5): 203-9. Doi: <https://doi.org/10.30880/ijie.2020.12.05.025>.
- [5] Dilberoglu, U. M., Simsek, S. and Yaman, U. 2019. Shrinkage Compensation Approach Proposed for ABS Material in FDM Process. *Materials and Manufacturing Processes*. 34(9): 993-8. Doi: <https://doi.org/10.1080/10426914.2019.1594252>.
- [6] Shirmohammadi, M., Goushchi, S. J. and Keshitban, P. M. 2021. Optimization of 3D Printing Process Parameters to Minimize Surface Roughness with Hybrid Artificial Neural Network Model and Particle Swarm Algorithm. *Progress in Additive Manufacturing*. 1-17. Doi: <https://doi.org/10.1007/s40964-021-00166-6>.
- [7] Mwema, F. M. and Akinlabi, E. T. 2020. *Fused Deposition Modeling: Strategies for Quality Enhancement*. Switzerland: Springer Nature. Doi: <https://doi.org/10.1007/978-3-030-48259-6>.
- [8] Snapp, K. L., Gongora, A. E. and Brown, K. A. 2021. Increasing throughput in Fused Deposition Modeling by Modulating Bed Temperature. *Journal of Manufacturing Science and Engineering*. 143(9): 094502-7. Doi: <https://doi.org/10.1115/1.4050177>.
- [9] Devicharan, R. and Garg, R. 2019. Optimization of the Print Quality by Controlling the Process Parameters on 3D Printing Machine. In: Kumar, L. J., Pandey, P. M., Wimpenny, D. I. (eds.). *3D Printing and Additive Manufacturing Technologies*. Singapore: Springer. 187-94. Doi: https://doi.org/10.1007/978-981-13-0305-0_16.
- [10] Schmutzler, C., Zimmermann, A. and Zaeh, M. F. 2016. Compensating Warpage of 3D Printed Parts using Free-Form Deformation. *Procedia CIRP*. 41: 1017-22. Doi: <https://doi.org/10.1016/j.procir.2015.12.078>.
- [11] Armillotta, A., Bellotti, M. and Cavallaro, M. 2018. Warpage of FDM Parts: Experimental Tests and Analytic Model. *Robotics and Computer-Integrated Manufacturing*. 50: 140-52. Doi: <https://doi.org/10.1016/j.rcim.2017.09.007>.
- [12] Kaushik, P. 2020. Introduction to Regression Analysis [using Excel] [Online]. *Towards Data Science*. Available: <https://towardsdatascience.com/introduction-to-regression-analysis-using-excel-398ae1c3d604>. [Accessed May 7th 2022].
- [13] Zaiontz, C. 2022. Real Statistics Resource Pack [Online]. *Real Statistics Using Excel*. <https://www.real-statistics.com/free-download/real-statistics-resource-pack/>. [Accessed May 7th 2022].
- [14] Quill, T. J., Smith, M. K., Zhou, T., Baioumy, M. G. S., Berenguer, J. P., Cola, B. A., Kalaitzidou, K. and Bougher, T. L. 2018. Thermal and Mechanical Properties of 3D Printed Boron Nitride – ABS Composites. *Applied Composite Materials*. 25(5): 1205-17. Doi: <https://doi.org/10.1007/s10443-017-9661-1>.
- [15] Smith, W., and Hashemi, J. 2022. *ISE Foundations of Materials Science and Engineering*. 7th ed. New York: McGraw Hill.
- [16] Yunus, A., Cimbala, J. and Afshin, G. 2021. *Fundamentals of Thermal-fluid Sciences*. New York: McGraw Hill.
- [17] Halliday, D., Resnick, R. and Walker, J. 2021. *Fundamentals of Physics*. New York: Wiley.
- [18] Rosli, A. A., Shuib, R. K., Ishak, K. M. K., Hamid, Z. A. A., Abdullah, M. K., Rusli, A. 2020. Influence of Bed Temperature on Warpage, Shrinkage and Density of Various Acrylonitrile Butadiene Styrene (ABS) Parts from Fused Deposition Modelling (FDM). *AIP Conference Proceedings*. 2267(020072): 1-10. DOI: <https://doi.org/10.1063/5.0015799>.
- [19] Sahay, C. and Ghosh, S. Understanding Surface Quality: Beyond Average Roughness (R_a). *2018 ASEE Annual conference & Exposition, Salt Lake City, US*. 23-27 June 2018. 1-20.
- [20] Pérez, M., Medina-Sánchez, G., García-Collado, A., Gupta, M. and Carou, D. 2018. Surface Quality Enhancement of Fused Deposition Modeling (FDM) Printed Samples based on the Selection of Critical Printing Parameters. *Materials*. 11(8): 1382. Doi: <https://doi.org/10.3390/ma11081382>.
- [21] Jo W., Kwon, O. -C and Moon M. -W. 2018. Investigation of Influence of Heat Treatment on Mechanical Strength of FDM Printed 3D Objects. *Rapid Prototyping Journal*. 24(3): 637-44. Doi: <https://doi.org/10.1108/RPJ-06-2017-0131>.
- [22] Jo, W., Lee, J. S., Lee, H. J. and Moon, M. -W. 2014. 3D Printed Tactile Pattern Formation on Paper with Thermal Reflow Method. *RSC Advances*. 4(60): 31764-31770. Doi: <https://doi.org/10.1039/C4RA02822H>.

APPENDIX A: REGRESSION ANALYSIS OF UP-SKIN'S MAXIMUM Z-DEFLECTION PLOTS

<i>Original Samples' Regression Statistics</i>					
Multiple R		0.5102163			
R Square		0.2603207			
Adjusted R Square		0.013761			
Standard Error		1.3955415			
Observations		5			
ANOVA					
	<i>df</i>	<i>SS</i>	<i>MS</i>	<i>F</i>	<i>Significance F</i>
Regression	1	2.05623161	2.056232	1.055812	0.3797758 > 0.05
Residual	3	5.84260794	1.947536		
Total	4	7.89883955			
<i>Zinc-overlaid Samples' Regression Statistics</i>					
Multiple R		0.7134899			
R Square		0.5090679			
Adjusted R Square		0.3454238			
Standard Error		0.8604423			
Observations		5			
ANOVA					
	<i>df</i>	<i>SS</i>	<i>MS</i>	<i>F</i>	<i>Significance F</i>
Regression	1	2.30313307	2.303133	3.110824	0.17596936 > 0.05
Residual	3	2.22108306	0.740361		
Total	4	4.52421613			

APPENDIX B: T-TEST ANALYSIS OF UP-SKIN'S MAXIMUM Z-DEFLECTION PLOTS

<i>t-Test: Two-Sample Assuming Unequal Variances</i>		
	<i>Original</i>	<i>Zinc-overlaid</i>
Mean	2.59064	2.07628
Variance	1.97471	1.131054032
Observations	5	5
Hypothesized Mean Difference	0	
df	7	
t Stat	0.652631	
P(T<=t) one-tail	0.267416 > 0.05	
t Critical one-tail	1.894579	
P(T<=t) two-tail	0.534831	
t Critical two-tail	2.364624	

APPENDIX C: REGRESSION ANALYSIS OF R_A ROUGHNESS PLOTS

<i>Original Samples' Regression Statistics</i>					
Multiple R	0.951119				
R Square	0.904627				
Adjusted R Square	0.872836				
Standard Error	0.277995				
Observations	5				
ANOVA					
	<i>df</i>	<i>SS</i>	<i>MS</i>	<i>F</i>	<i>Significance F</i>
Regression	1	2.199069	2.199069	28.45549	0.012878 < 0.05
Residual	3	0.231843	0.077281		
Total	4	2.430912			
<i>Zinc-overlaid Samples' Regression Statistics</i>					
Multiple R	0.903311				
R Square	0.81597				
Adjusted R Square	0.754627				
Standard Error	0.311508				
Observations	5				
ANOVA					
	<i>df</i>	<i>SS</i>	<i>MS</i>	<i>F</i>	<i>Significance F</i>
Regression	1	1.290766	1.290766	13.30173	0.035563 < 0.05
Residual	3	0.291112	0.097037		
Total	4	1.581878			

APPENDIX D: REGRESSION ANALYSIS OF R_Z ROUGHNESS PLOTS

<i>Original Samples' Regression Statistics</i>	
Multiple R	0.915305
R Square	0.837783

Adjusted R Square	0.783711
Standard Error	1.197794
Observations	5

ANOVA

	<i>df</i>	<i>SS</i>	<i>MS</i>	<i>F</i>	<i>Significance F</i>
Regression	1	22.22909	22.22909	15.49379	0.02921 < 0.05
Residual	3	4.304129	1.43471		
Total	4	26.53322			

Zinc-overlaid Samples' Regression Statistics

Multiple R	0.826253
R Square	0.682693
Adjusted R Square	0.576924
Standard Error	1.924144
Observations	5

ANOVA

	<i>df</i>	<i>SS</i>	<i>MS</i>	<i>F</i>	<i>Significance F</i>
Regression	1	23.89697	23.89697	6.454574	0.084636 > 0.05
Residual	3	11.10699	3.702331		
Total	4	35.00396			